ACS Catalysis

Research Article

pubs.acs.org/acscatalysis

Fischer–Tropsch Synthesis: Higher Oxygenate Selectivity of Cobalt Catalysts Supported on Hydrothermal Carbons

Uschi M. Graham, Gary Jacobs, Muthu K. Gnanamani, Stephen M. Lipka, Wilson D. Shafer, Christopher R. Swartz, Thani Jermwongratanachai, Rong Chen, Fon Rogers, and Burtron H. Davis*

Center for Applied Energy Research, University of Kentucky, 2540 Research Park Drive, Lexington, Kentucky 40511, United States

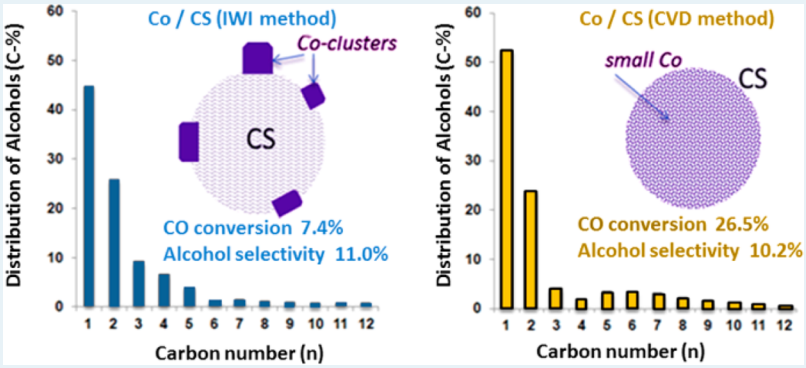

ABSTRACT: The performance of carbon-supported cobalt catalysts was compared with that of Co/γ-Al_2O_3 reference catalysts for the Fischer–Tropsch synthesis (FTS) reaction. The carbon support (CS) was prepared using a hydrothermal method that formed mostly spherical ~300–800 nm carbons that were first carbonized at 900 °C and then partially graphitized at 1900 °C. The FTS study was conducted using a continuously stirred tank reactor, and the cobalt catalysts were promoted with Pt (0.2% Pt–10% Co) to facilitate the reduction of cobalt oxides. Catalysts were prepared by an evaporative method (Co/CS-IWI) and by a chemical vapor deposition technique (Co/CS-CVD). The CVD technique led to a higher CO conversion (26.5%) relative to the conventional evaporative (IWI) method (7.4%) at the same temperature (220 °C) and space velocity (1.5 NL/g_{cat}h). Remarkably, the Co/CS-CVD displayed a high oxygenate selectivity (~10%) in comparison with cobalt alumina catalysts (i.e., including one having similar Pt and Co loadings, as well as a conventional cobalt alumina catalyst with a higher Co loading of 25% Co) at similar conversion levels. The difference in the CO conversion on a per gram catalyst basis observed between Co/CS-IWI and Co/CS-CVD catalysts was due to the smaller average Co particle size and more uniform distribution resulting from the CVD method.

KEYWORDS: *hydrothermal process, carbon spheres, cobalt, Fischer–Tropsch synthesis, oxygenates, chemical vapor deposition, HR-TEM, X-ray absorption spectroscopy*

1. INTRODUCTION

Synthesis gas, a mixture of carbon monoxide and hydrogen (H_2/CO) can be converted into hydrocarbons using cobalt (Co) catalysts during Fischer–Tropsch synthesis (FTS). Cobalt is well-known for its activity in FTS and is typically supported on metal oxides, such as Al_2O_3, TiO_2, or SiO_2. Extensive efforts have been made to develop FTS catalysts with high activity and high C_{5+} selectivity,[1,2] and the prospect of using ordered porous carbon materials as supports for Co catalysts was introduced to minimize, and ideally bypass, the catalyst–support interactions typically encountered for small cobalt particles on metal oxides.[3] Carbon support structures have been shown to influence the reactivity and product distribution during FTS, and for Co catalysts, the activities using various mesoporous carbon supports were previously assessed.[4] Carbon support structures are an appealing alternative to metal oxides because the surfaces can be manipulated with appropriate surface functionalization, and surface areas can be greatly enhanced through physical and chemical treatments;[5] however, there are great variations in carbon support materials, including fibers, nanotubes, nanowires, and molecular sieves, just to mention a few, and they may produce different outcomes for FTS.[6] The current study focuses on hydrothermally derived carbon spheres as a support for Co nanoparticles.

Carbonaceous materials made from the hydrothermal process are unique in that properties such as microstructure, surface functionality, size, morphology, chemical composition, surface area, and micro- and meso-porosity can be tailored by the selection of the carbohydrate precursor and synthetic growth conditions. The hydrothermal synthesis (HTS) process for generating carbonaceous materials in the form of nano- and

Received: October 23, 2013
Revised: April 10, 2014
Published: April 11, 2014

   dx.doi.org/10.1021/cs400965t | ACS Catal. 2014, 4, 1662–1672

microspheres can use mono- and polysaccharides[7−10] or industrial biomass waste derivatives. Hydrothermal techniques are a particular case of solvothermal processes that operate on the principle of small crystals growing from solution at high pressures and high temperatures. The hydrothermal method is a "greener" synthetic approach because no toxic organic solvents, initiators, or surfactants are used that commonly were components of carbon spheres.[11] A traditional hydrothermal synthesis method is typically carried out in an autoclave type reactor, where an aqueous solution is heated slowly to a certain temperature and then aged for several hours or days at supercritical water and near-critical water conditions. The method produces submicro- and nanometer-sized carbon spheres without additional physical and chemical reaction steps. HTS also has the advantage of reduced contamination and low energy consumption. Material characteristics such as particle size, morphology, and size distribution can be controlled to some extent by independently varying the temperature, pressure, and concentration of reactants and flow rates if a continuous process is used.[12] The mild temperatures (typically <250 °C) and versatility of HTS can enable detailed control of monodispersity, chemical composition, and also the microscopic structure of carbonaceous materials. The carbons can then be physically or chemically treated to generate desired pore structures and crystallinity. This leads to new frontiers in catalyst supports through the use of tailor-made carbon spheres.

Hydrothermal carbons typically have oxygen functional groups in surface layers,[12] and a potential effect on oxygenate formation during FTS needs to be investigated, since the nature of the support is known to affect the catalytic activity and selectivity of cobalt catalysts.[13−16] Oxygenates in fuel blends are significant during combustion by effectively delivering oxygen to the pyrolysis zone of a burning fuel and result in reduced particle matter generation.[17] Many mechanisms for oxygenate formation during FTS have been suggested and are summarized elsewhere,[16] and this study aims to provide further insights into the importance of hydrothermally derived carbon support surfaces. The catalyst particles were prepared on the carbon support either by an incipient wetness impregnation (IWI) method or by a chemical vapor deposition (CVD) method with the goal of having two distinct catalyst particle sizes to compare. Moreover, the catalyst selectivities were compared to Pt promoted Co/alumina reference catalysts, including one with identical Pt and Co loadings.

2. EXPERIMENTAL SECTION

2.1. Carbon Support Preparation. Xylose (37.5 g) and anhydrous phloroglucinol (31.5 g) were dissolved in 1 L of DI water, and the solution was added to a Teflon-lined pressure vessel (Parr Instruments) and heated to 200 °C for 12 h. After cooling to ambient temperature, the solid product was collected by filtration. The carbon spheres were mixed with isopropyl alcohol and then blended by a high-shear mixer (Silverson L5M-A) at 9000 rpm for 30 min to break up agglomerates. The solids were dried in a vacuum oven at 120 °C for 24 h (45 g of solid product was collected per run). The dry carbon spheres were carbonized at 1000 °C for 1 h in nitrogen with a mass loss of 51%. The carbon spheres were then partially graphitized in He at 1900 °C for 1 h with a mass loss of 0.5%, and the resulting carbon support was termed CS.

2.2. Catalyst Preparation. *(a). Method I: Evaporative Deposition (IWI).* The CS-supported cobalt catalyst (0.2% Pt−10% Co/C) was prepared by following the evaporative deposition technique[18] using CS powder and a solution of cobalt nitrate (cobalt nitrate hexahydrate, $Co(NO_3)_2{\cdot}6H_2O$, Sigma-Aldrich, 99.95%). Typically, 15.0 g of dry CS was immersed in 8.23 g of $Co(NO_3)_2{\cdot}6H_2O$ and dissolved in a 4:1 mixture of toluene and ethanol. About 2 mL of deionized water were added to the toluene and ethanol mixture to dissolve the cobalt nitrate salts completely. The excess solvent was then removed by vacuum evaporation at 80 °C. Afterward, 0.0597 g of tetraamine platinum(II) nitrate were introduced to the dried catalyst by following the same evaporative deposition technique as describe above to achieve a promoter loading of 0.2 wt %. Finally, the promoted catalyst material was dried at 120 °C overnight and calcined under N_2 flow at 350 °C for 4 h.

For the 0.2% Pt−0% Co/Al_2O_3 reference catalyst, cobalt was added to Catalox 150 γ-alumina by the conventional slurry phase impregnation method[19] such that 2.5 times the pore volume was used to calculate the volume of the loading solution of aqueous cobalt nitrate. Following drying in a rotary evaporator between 80 and 100 °C, 0.2% of Pt was added by incipient wetness impregnation of tetraamine platinum(II) nitrate. After a second drying step using the rotary evaporator, the catalyst was calcined in flowing air at 350 °C for 4 h. CAER has previously reported results on a 0.5% Pt−25% Co/Al_2O_3 catalyst (BET SA = 97.8 m^2/g, % reduced = 64.1%, corrected Co metal diameter = 12.3 nm) for gas-to-liquids testing, and the preparation procedure is the same as above, except that multiple impregnation and drying steps were required to load $Co(NO_3)_2$ as a result of the solubility limit. The average cobalt diameter and extent of reduction were determined by hydrogen chemisorption/pulse reoxidation.[36] After reducing the 0.2% Pt−10% Co/Al_2O_3 catalyst at 350 °C for 10 h and cooling to 80 °C, the amount of H_2 evolved from TPD to 350 °C was 75.6 μmol/g, and the uptake of O_2 at 350 °C was 884.5 μmol/g. Thus, the extent of reduction was 78.2%, the corrected dispersion (i.e., taking into account the percent reduction) was 11.4%, and the average Co metal cluster diameter was 9.1 nm.

(b). Method II: Chemical Vapor Deposition. The CS sample was treated in flowing N_2 (100 cm^3/min) at 350 °C for 4 h. After cooling, the CS powder was transferred to a glovebag filled with inert gas, carefully mixed with cobalt and platinum acetylacetonates (Alfa Aesar), and loaded into sublimation tubes, which were sealed at one end. The other end was attached to a high vacuum system, equipped with an oil diffusion pump and capable of achieving a vacuum of $<10^{-6}$ Torr. The sublimation tube was then held at ambient temperature for 4 h and slowly ramped (1 °C/min) to 60 °C and then to 100 °C (at 0.25 °C/min), holding at each temperature for 1 h. Finally, the temperature was ramped to 130 °C (1 °C/min), held for 15 min, and cooled to room temperature. To decompose the cobalt and platinum acetylacetonate compounds, the catalyst was again treated in flowing nitrogen for 4 h at 350 °C. The loading was 0.2% of Pt and 10% Co by weight. Various sublimation methods for obtaining highly dispersed catalysts by CVD can be found in the literature.[20−26]

2.3. Standard Catalyst Characterization Methods. Cobalt and platinum elemental analysis and loadings on the catalyst support for both IWI and CVD catalysts were determined by inductively coupled plasma optical emission spectroscopy using a Varian 720-ES analyzer. The materials were dissolved in a percholoric/nitric acid mixture and the

dx.doi.org/10.1021/cs400965t | ACS Catal. 2014, 4, 1662−1672

Table 1. Activity and Selectivity of the FTS Reaction for Carbon-Supported Cobalt Catalysts[a]

			selectivity (%)		carbon distribution (%)			α-value[b]	
catalyst	CO conv. (%)	temp (°C)	CH_4	CO_2	paraffin	olefin	alcohol	α_{CH}	α_{OH}
Co/CS-IWI[c,d]	7.4	220	15	0.7	71.0	18.0	11.0	0.76	0.60
Co/CS-CVD[d,e]	26.5	220	18	1.7	77.4	13.2	10.2	0.66	0.60
	38.3	220	18	1.4	79.5	11.7	7.8	0.70	0.64
Co/Al_2O_3[f]	22.2	220	9.4	0.6	74.3	18.8	5.3	0.84	0.56
	37.0	220	6.7	0.6	75.1	17.6	5.5	0.85	0.71
Co/Al_2O_3[g]	21.3	220	8.1	0.2	80.0	17.2	2.4	0.82	–

[a]Reaction conditions: 220 °C, 2.0 MPa, H_2/CO = 2.0, SV = 1.5. [b]Chain growth probability factor calculated for carbon numbers in the range of C_2–C_{16}. [c]Co/CS-IWI: 0.2% Pt–10% Co. [d]TOS for Co/CS-IWI and Co/CS-CVD was 150 h. [e]Co/CS-CVD: 0.2% Pt–10% Co. [f]0.2% Pt–10% Co/Al_2O_3-impregnated (220 °C, 2.0 MPa, H_2/CO = 2.0, SV = 3.0; TOS 95.5 h). [g]A standard alumina catalyst: 0.5% Pt–25% Co/γ-Al_2O_3 (220 °C, 2.0 MPa, H_2/CO = 2.0, SV = 15.0; TOS 150 h).

emission spectra of dissolved species (Co, Pt) were compared with those of a series of standard solutions of known concentrations.

A powder X-ray diffraction (XRD) study was performed on calcined catalysts using a Philips X'pert diffractometer using monochromatic Cu Kα radiation (λ = 1.5418 Å). A scan rate of 0.01° per step and a scan time of 90 s per step over a 2θ range of 10–80° were used. The particle size of Co_3O_4 was calculated from the line broadening of a Co_3O_4 line (2θ of 36.8°).

BET surface area and porosity measurements of the carbon support and freshly prepared catalysts were conducted using a Micromeritics Tri-Star system. Before performing the test, the temperature was gradually ramped to 160 °C, and the sample was evacuated for at least 12 h at ~50 mTorr. The BET surface area, pore volume (single point), and average pore radius (single point and BJH adsorption) were obtained for each sample.

Temperature-programmed reduction (TPR) profiles of freshly prepared catalysts were recorded using a Zeton-Altamira AMI-200 unit equipped with a thermal conductivity detector (TCD). The TPR was performed using a 10% H_2/Ar gas mixture and referenced to argon at a flow rate of 30 cm^3/min. The sample was heated from 50 to 800 °C using a heating ramp of 10 °C/min.

X-ray photoelectron spectroscopy analysis (XPS) was performed using a VG Scientific MultiLab 3000 ultrahigh vacuum surface analysis system (operating at a base pressure in the 10^{-8} Torr range) equipped with a dual-anode (Mg/Al) X-ray source and a CLAM4 hemispherical electron energy analyzer. The source was a nonmonochromatized Mg Kα X-ray beam ($h\nu \approx$ 1253.6 eV). Spectra were collected at an electron emission angle of 54.7° relative to the surface normal, and high resolution spectra were collected with a PAS energy of 50 eV.

2.4. HR-TEM Imaging. High resolution transmission electron microscopy (HRTEM) imaging was performed using a FEI Tecnai F20 field-emission gun (accelerating voltage of 200 kV) and symmetrical multibeam illumination with a Gatan Ultrascan CCD camera. Data processing and analysis were carried out using the Gatan Digital Micrograph software. Samples were prepared on lacy carbon copper grids and dispersed as powders.

2.5. XANES/EXAFS Measurements. X-ray absorption spectroscopy (XAS) on reference compounds and freshly activated 0.2% Pt–10% Co/C catalyst samples prepared by either CVD or IWI was conducted at Brookhaven National Laboratory (Beamline X-18b). The beamline was equipped with a Si(111) channel cut monochromator. A crystal detuning procedure was used to remove harmonic content from the beam and make the relative response of the incident and transmission detectors more linear. The X-ray intensity was ~1 × 10^{10} photons/s, and the usable energy range was from 4.8 to 40 keV. EXAFS/XANES spectra were recorded in transmission mode near the Co K edge. Sample thickness was determined by calculating the amount in grams per square centimeter of sample (w_D) by utilizing the following thickness equation:

$$w_D = \ln(I_0/I_t)/\sum\{(m/r)_j w_j\} \quad (1)$$

where m/r is the total cross section (absorption coefficient/density) of element "j" in the sample at the absorption edge of the EXAFS element under consideration (units, $cm^2\ g^{-1}$), w_j is the weight fraction of element j in the sample and $\ln(I_0/I_t)$ was taken over a typical range of 1–2.5. Wax was utilized to fix the sample in the activated state (i.e., after H_2 reduction for 10 h at 350 °C) and such that a pellet could be formed. In addition, the pellet was sealed from ambient air. Smooth self-supporting pellets, free of pinholes, were loaded into the XAS cell. EXAFS data reduction and fitting were carried out using the WinXAS,[28] Atoms,[29] FEFF,[30] and FEFFIT[30] programs. The k and r ranges for fittings were chosen to be 3–13 $Å^{-1}$ and 1.5–3 Å, respectively. The CoO reference for XANES was obtained from the TPR trajectory of a 15% Co/Al_2O_3 catalyst, at the point of maximum CoO content.[31]

2.6. Fischer–Tropsch Synthesis. FTS was performed using a 1 L CSTR. In a typical experiment, 20 g of calcined catalyst (80–140 mesh) was reduced ex situ using a H_2/He (1:3) mixture at 350 °C for 15 h. The reduced catalyst was transferred to a 1 L CSTR, which already contained 310 g of melted Polywax 3000 (polyethylene with average carbon number of 200) under flowing nitrogen. The catalyst was further reduced in situ using pure H_2 (30 SL/h) at 230 °C for 24 h as a precautionary measure. The FTS reaction was conducted at a temperature of 220 °C and a syngas pressure of 2.0 MPa with varying space velocities (2.0, 1.0, 0.4, and 0.2 SL/h/g cat) and at a constant H_2/CO of 2:1.

To analyze the FTS products, effluent gases were analyzed online using a Micro GC (HP, Quad series, Refinery Gas analyzer) equipped with a TCD, while the liquid products condensed in the 273 and 373 K traps were analyzed separately. A HP 5890 GC with DB-5 capillary column was employed for oil and wax analysis, and a HP 5790 GC with Porapak Q packed column was used for water analysis. A 5973N MSD coupled to the 6890 GC from Agilent was employed for qualitative analysis of oxygenates, which were further quantified using a FID. The FID response factor for hydrocarbons is considered to be 1.0, and it was corrected for oxygenates using

dx.doi.org/10.1021/cs400965t | ACS Catal. 2014, 4, 1662–1672

a reported value.[27] The conversion and selectivity parameters are defined as

$$\%\text{CO conversion} = 100 \times \frac{n\text{CO}_{\text{in}} - n\text{CO}_{\text{out}}}{n\text{CO}_{\text{in}}}$$

$$\text{selectivity}(\%) = 100 \times \frac{n_{\text{product out}} \cdot \text{carbon number}}{n\text{CO}_{\text{in}} - n\text{CO}_{\text{out}}}$$

where $n\text{CO}_{\text{in}}$ and $n\text{CO}_{\text{out}}$ are the number of moles of CO fed and not consumed, respectively. The selectivity is defined as the percentage of moles of CO consumed to form a particular C_n product (hydrocarbon, CO_2, or oxygenate), normalized by the amount of CO consumed.

3. RESULTS AND DISCUSSION

3.1. FTS: Catalysis. The FTS study was conducted using a 1L CSTR with Pt (0.2%)−Co (10%) catalysts that were supported on partially graphitized (1900 °C) carbon spheres (CS), as well as Pt-promoted cobalt alumina reference catalysts. Details of the reactor setup conditions and performance criteria are summarized in ref 32. Catalysts on the CS were prepared either by IWI (Co/CS-IWI) or CVD (Co/CS-CVD). Fischer−Tropsch synthesis experiments were performed at 220 °C, and the pressure was kept at 2.0 MPa at a constant H_2/CO ratio of 2.0. The CO conversion and the product selectivity as well as the carbon distribution and alpha values of the two different cobalt catalysts (Co/CS-IWI vs Co/CS-CVD) were compared with the two Pt-promoted cobalt alumina catalysts (Pt−Co/γ-Al_2O_3), as shown in Table 1. The cobalt alumina catalysts include a catalyst having Pt and Co loadings identical to the Co/CS catalysts, as well as a conventional catalyst with a higher Co loading. Co/CS-IWI displayed a CO conversion of 7.4%, which is significantly lower than the value of 26.5% observed for the Co/CS-CVD catalyst. Because the SV was much higher (i.e., 15) for the 0.5% Pt−25% Co/Al_2O_3 catalyst, the hydrocarbon production rate is higher on a per-gram catalyst

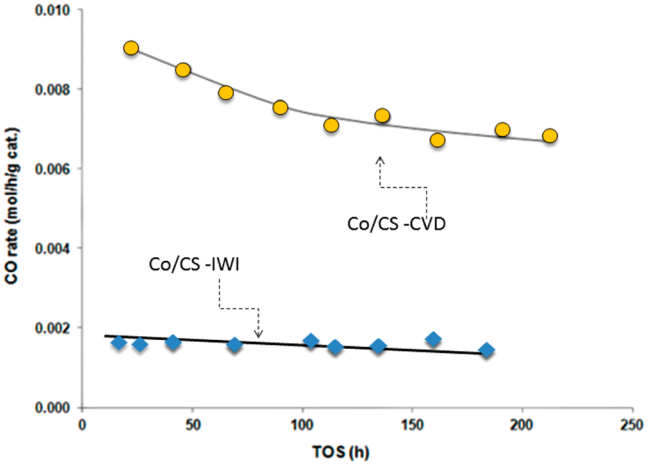

Figure 1. FTS performance of carbon-supported cobalt catalysts (0.2% Pt−10% Co/CS) prepared by IWI and CVD methods (reaction conditions: 220 °C, 2.0 MPa, H_2/CO = 2.0, SV = 1.5).

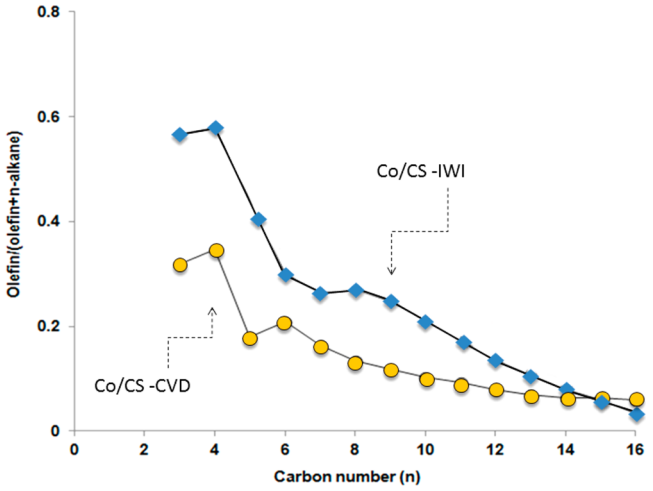

Figure 3. Selectivity to olefins as a function of carbon number for carbon supported cobalt FT catalysts (reaction conditions: 220 °C, 2.0 MPa, H_2/CO = 2.0, SV = 1.5).

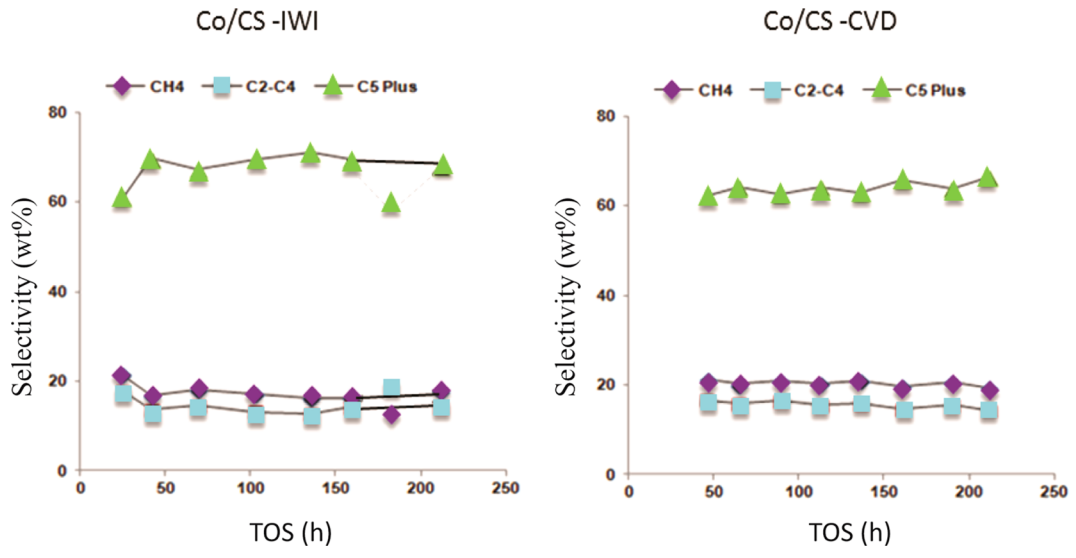

Figure 2. Change of selectivity with time-on-stream for FT synthesis of carbon supported cobalt catalysts prepared by IWI and CVD methods (reaction conditions: 220 °C, 2.0 MPa, H_2/CO = 2.0, SV = 1.5). Note differences in CO conversion levels for the two catalysts.

dx.doi.org/10.1021/cs400965t | ACS Catal. 2014, 4, 1662−1672

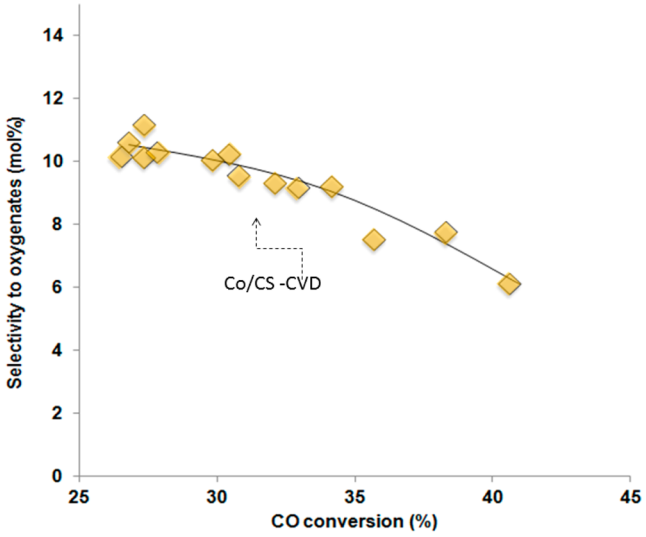

Figure 4. Dependency of oxygenates selectivity on CO conversion during FTS. Co catalyst prepared on hydrothermal carbon support (CS) using CVD technique.

Scheme 1. Formation Routes of Oxygenates in FT Synthesis[a]

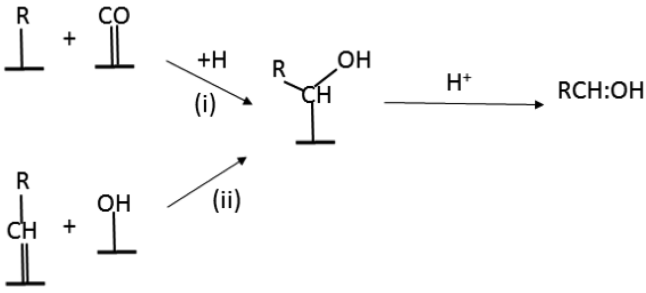

[a](i) CO insertion and (ii) addition of a hydroxyl group to an alkylidene species.

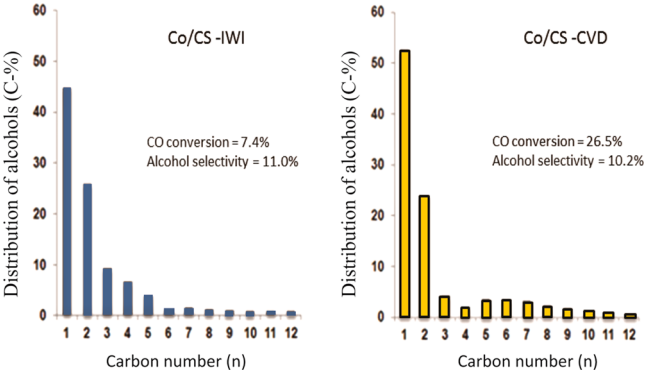

Figure 5. Distribution of alcohols among oxygenates for various carbon-supported cobalt FT catalysts (reaction conditions: 220 °C, 2.0 MPa, H_2/CO = 2.0, SV = 1.5).

basis. This is due in part to the higher loading of cobalt. Thus, a comparison was made with a Co/alumina catalyst having similar Pt and Co loadings. In that case, the SV was double that of the Co/CS catalysts and the conversion rate was also found to be higher (i.e., 37%). Thus, the hydrocarbon production rate was also higher for the 0.2% Pt−10% Co/alumina catalyst relative to either of the two Co/CS catalysts. Catalyst

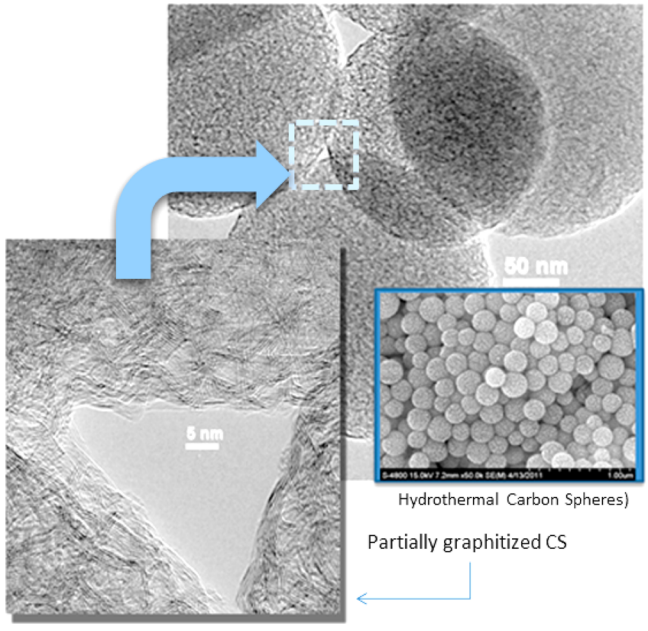

Figure 6. Hydrothermally synthesized carbon spheres (CS). The CS powders were partially graphitized at 1900 °C, and the resulting carbon nanostructures resemble ribbons that are made up of aligned carbon planes on the CS surfaces.

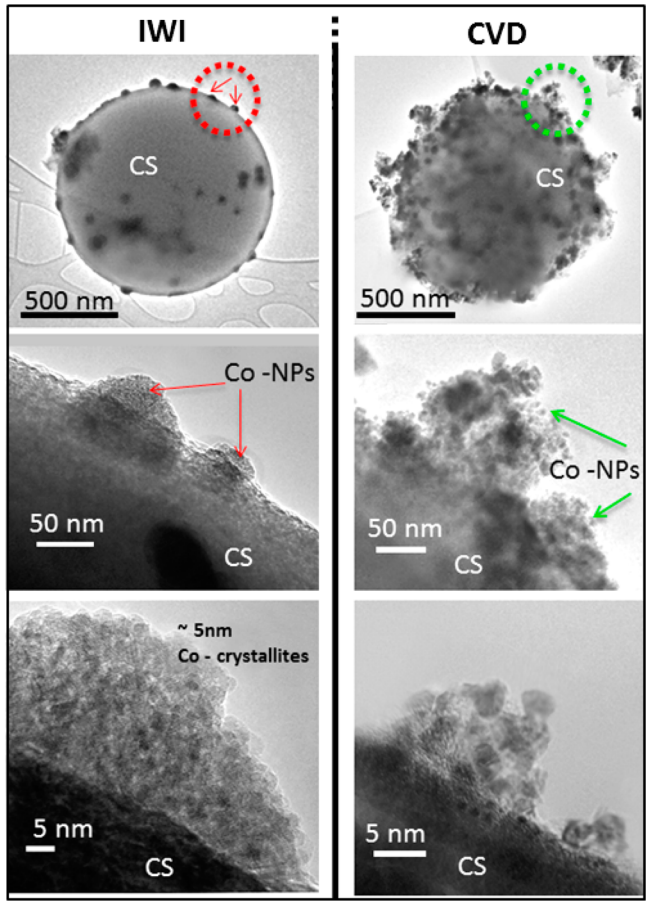

Figure 7. TEM images of CS with cobalt catalyst particles prepared by IWI (left column) and CVD (right column methods, before FTS).

performance was also evaluated in terms of the rate of conversion of CO in moles/hour/gram of catalyst versus time

dx.doi.org/10.1021/cs400965t | ACS Catal. 2014, 4, 1662−1672

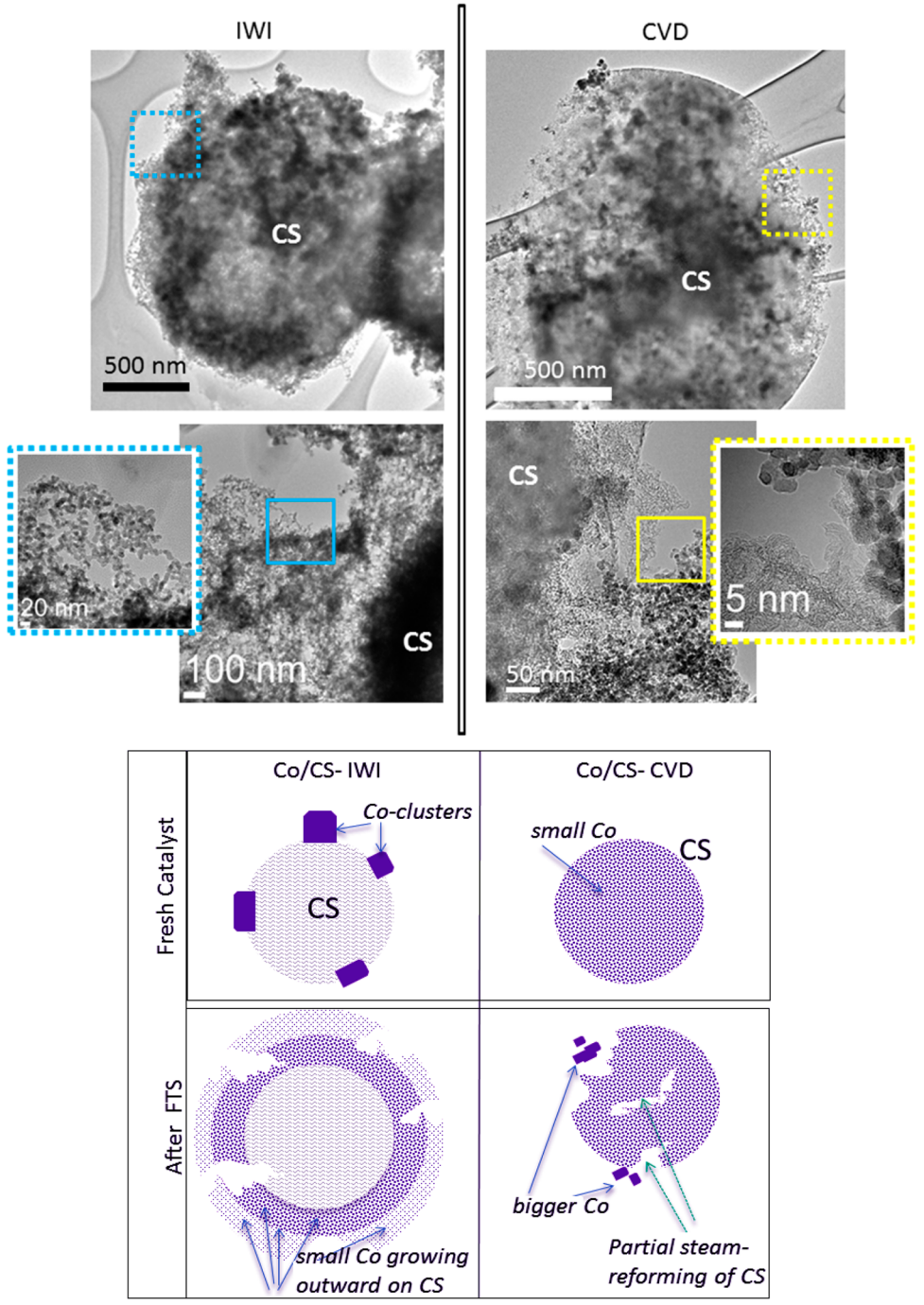

Figure 8. Comparison of IWI (left column) and CVD (right column) methods for Co on carbon spheres: TEM images shown catalyst after FTS. Schematic illustrates the unexpected particle size reduction for the IWI-prepared catalyst: Large Co clusters disappear, and finely dispersed small Co cover the carbon support (CS). The CVD-sample starts with small Co dispersed throughout the CS support, and after FTS, only some larger Co clusters appear while portions of the CS support are vaporized (during partial steam reforming of the carbon support).

on-stream (Figure 1). The Co/CS-CVD catalyst displayed a higher CO conversion rate relative to the Co/CS-IWI catalyst over the entire testing period; the activity of the CVD catalyst became stable after 100 h of FT synthesis. Since the Co/CS-IWI and Co/CS-CVD catalysts were prepared by using the same carbon support material, the difference in the activity observed between these two catalysts must be due to the difference in the preparation methods (IWI vs CVD). The selectivity of the Co/CS-CVD catalyst was compared with both the standard alumina supported cobalt catalyst (0.5% Pt−25% Co/Al_2O_3), as well as the Pt−Co/alumina catalyst prepared with identical Pt and Co loadings (0.2% Pt−10% Co/Al_2O_3), at similar conversion levels. Results are provided in Table 1. The main finding is that the Co/CS-CVD catalyst exhibits much higher oxygenates selecitivity compared with either of the two Pt−Co/alumina reference catalysts at similar CO conversion levels.

Catalyst selectivities to light hydrocarbons (i.e., CH_4 as well as C_2−C_4) and heavier hydrocarbons (C_{5+}) are shown in Figure 2 for the IWI and CVD prepared carbon supported catalysts. Both have similar methane (~20%) and C_2−C_4 selectivity, and their C_{5+} selectivities are in the range of 60−70%. However,

dx.doi.org/10.1021/cs400965t | ACS Catal. 2014, 4, 1662−1672

Table 2. BET Surface Area and Porosity Results

sample	BET SA (m^2/g)	single-point pore volume (cm^3/g)	BJH adsorption pore volume (cm3/g)	BJH desorption pore volume (cm3/g)	single-point average pore radius (nm)	BJH adsorption average pore radius (nm)	BJH desorption average pore radius (nm)
Catalox 150 γ-Al_2O_3	149.3	0.493	0.500	0.499	6.9	5.4	4.8
0.2% Pt−10% Co/γ-Al_2O_3	124.1	0.342	0.355	0.354	5.5	5.0	4.5
graphitized carbon	3.25	0.0059	0.0074	0.0074	7.3	9.2	8.7
0.2% Pt−10% Co/C (IWI)	24.0	0.0564	0.0547	0.0551	4.8	6.9	6.5
0.2% Pt−10% Co/C (CVD)	16.4	0.0212	0.0211	0.0211	2.6	6.0	5.4

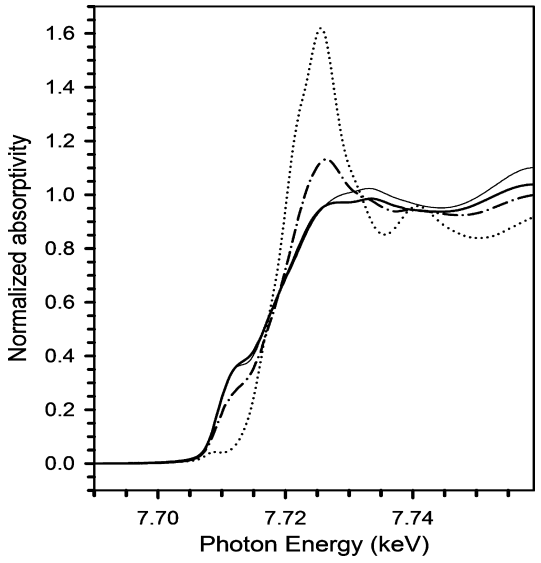

Figure 9. Normalized XANES spectra of (light solid line) Co metal foil; (heavy solid line) freshly reduced 0.2% Pt−10% Co/CS- IWI catalyst (heavy dash-dotted line) 0.2% Pt−10% Co/CS- CVD catalyst; and (dotted) the CoO reference.

note that direct comparisons of selectivity can be made only at similar conversion levels.

For both the IWI and CVD Co/CS catalysts, the percentage of olefinic content decreases with increasing carbon number (Figure 3). Again, a direct comparison of selectivities between the two catalysts cannot be made, since the conversion levels were significantly different. However, Table 1 shows that the total olefin + alcohol selectivities for the 0.2% Pt−10% Co/CS (CVD) and 0.2%−10% Co/Al_2O_3 catalysts at similar conversion levels were very close (23.4 versus 24.1, respectively). The results suggest a trade-off between olefin and alcohol selectivity between the two catalysts.

The chain growth probability factors (α) for hydrocarbons and alcohols produced from FT synthesis are also shown for the two hydrothermal carbon-supported (CS) catalysts (Table 1). The Co/CS −IWI catalyst exhibited a chain growth probability factor for hydrocarbons of 0.76, whereas that of the Co/CS −CVD was 0.66; note the difference in CO conversion levels, such that a direct comparison cannot be made. However, the CVD catalyst displayed a lower α value than either of the two Co/alumina reference catalysts (0.5% Pt−25% Co/Al_2O_3 had an α of 0.82; the 0.2% Pt−10% Co/Al_2O_3 catalyst had an α of 0.85) for hydrocarbons at similar conversion levels. The

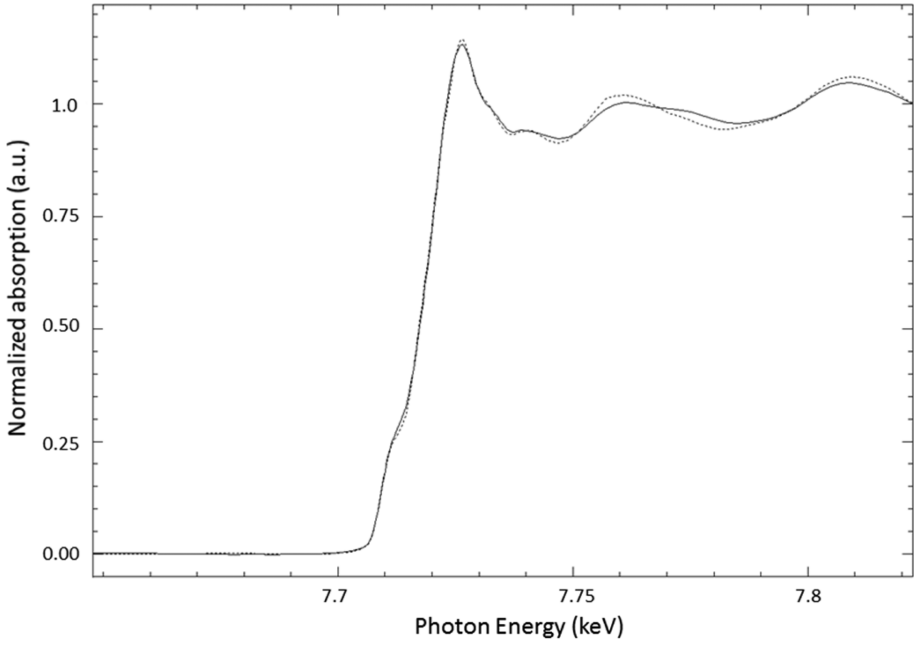

Figure 10. Linear combination XANES fitting of 0.2% Pt−10% Co/CS-CVD catalyst with CoO and Co metal foil reference compounds. The data were fitted over the range 7.69−7.76 keV (an excellent fitting was obtained with a residual of 1%).

dx.doi.org/10.1021/cs400965t | ACS Catal. 2014, 4, 1662−1672

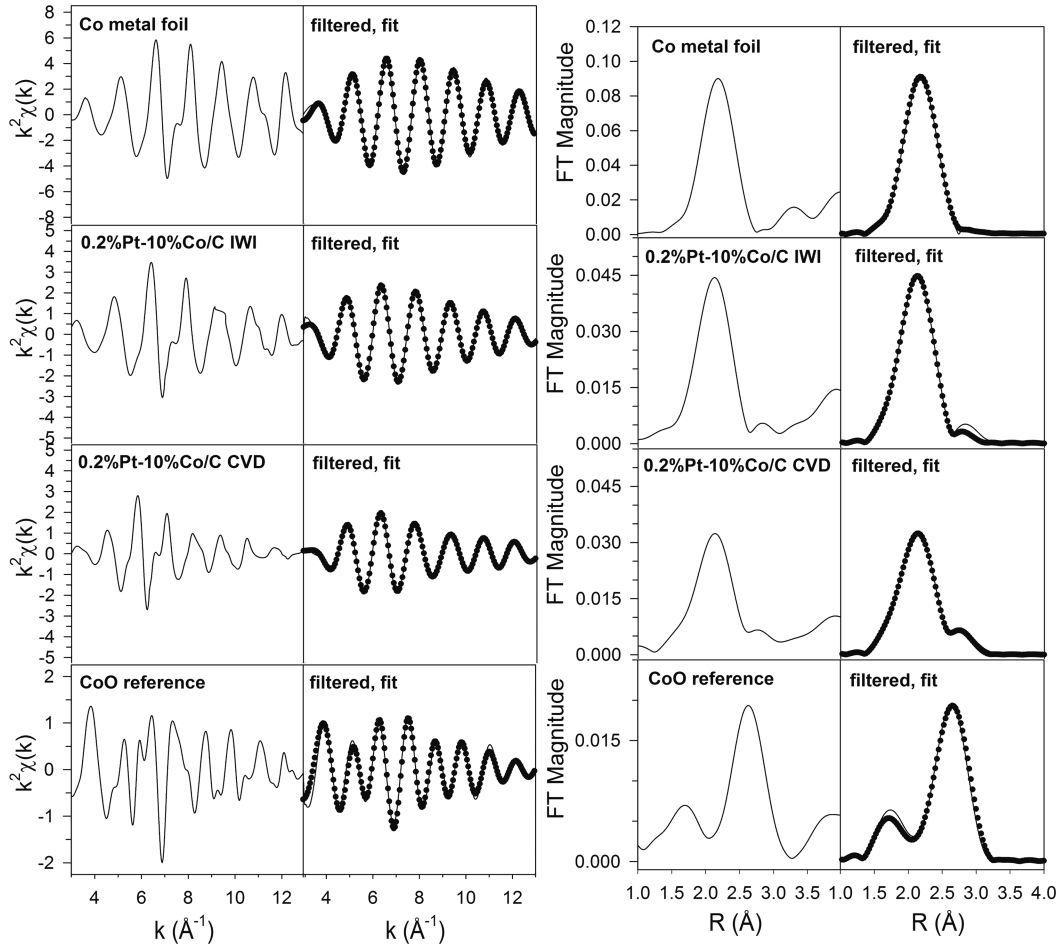

Figure 11. EXAFS fittings for the carbon supported catalysts: Note that although the catalyst samples have matching scales for the sake of direct comparison, the spectra of references do not. EXAFS results at the Co K-edge for (top) Co metal foil; (2nd from top) freshly activated 0.2% Pt−10% Co/CS-IWI catalyst after H_2 reduction at 350 °C; (2nd from bottom) the 0.2% Pt−10% Co/CS- CVD catalyst after H_2 reduction at 350 °C; and (bottom) a CoO reference compound, including the raw k^2 weighted $\chi(k)$ versus k, (middle) the filtered $\chi(k)$ versus k, and (dotted) the fitting; and (right) the raw Fourier transform magnitude spectrum and the filtered spectrum and (dotted) result of the fitting.

Table 3. Results of EXAFS Fitting Parameters for References Acquired near the Co K Edge[a]

sample description	N Co−O in CoO	R Co−O in CoO (Å)	N Co−Co in Co^0	R Co−Co in Co^0 (Å)	N Co−Co in CoO	R Co−Co in CoO (Å)	e_0 (eV)	σ^2 (Å^2)	r factor
Co metal			**12 (set)**	2.491 (0.0042)			7.97 (0.837)	0.00334 (0.00021)	0.0087
CoO powder reference	2.6 (0.5)	2.103 (0.019)			6.5 (1.0)	3.014 (0.010)	1.48 (1.40)	0.00686 (0.00130)	0.024
0.2% Pt−10% Co/C prepared by CVD	1.0 (0.2)	2.038 (0.031)	6.1 (0.5)	2.507 (0.0051)	2.1 (0.3)	3.043 (0.014)	−0.866 (0.890)	0.00580 (0.00061)	0.0049
0.2% Pt−5% Co/C prepared by IWI	0.5 (0.2)	2.026 (0.091)	7.8 (0.7)	2.498 (0.0054)	1.0 (0.5)	3.051 (0.033)	−2.15 (1.01)	0.00511 (0.00064)	0.0060

[a]The fitting ranges were Δk = 3−13 Å^{-1} and ΔR = 1.5−3.1 Å. S_0^2 was set to 0.9.

carbon distributions obtained for Co/CS-IWI and Co/CS-CVD catalysts (based on the gaseous and liquid hydrocarbons produced) are presented in Table 1, and oxygenates (i.e., primarily alcohols) make up a significant fraction of the products.

For the conventional 0.5% Pt−25% Co/Al_2O_3 catalyst, the FT hydrocarbon products contained ∼80% of linear paraffinic hydrocarbons, 17.2% olefins and 2.4% of alcohols at a CO conversion of 21.3%. For the 0.2% Pt−10% Co/Al_2O_3 catalyst, the FT hydrocarbon products contained 75.1% of linear paraffins, 17.6% olefins, and 5.5% alcohols (the latter with an α_{OH} of 0.71) at a CO conversion of 37.0%. At a lower conversion level of 22.2%, the FT hydrocarbons products contained 74.3% of linear paraffins, 18.8% of olefins, and 5.3% of alcohols. Only the CVD catalyst displayed a high enough conversion for direct comparison with the cobalt/alumina catalysts. In that case, at a conversion of 26.5%, the oxygenate selectivity was ∼4 times higher than the standard 0.5% Pt−25% Co/alumina catalyst (at X_{CO} = 21.3%), and still about double that of the 0.2% Pt−10% Co/Al_2O_3 catalyst (at X_{CO} = 22.2%).

dx.doi.org/10.1021/cs400965t | ACS Catal. 2014, 4, 1662−1672

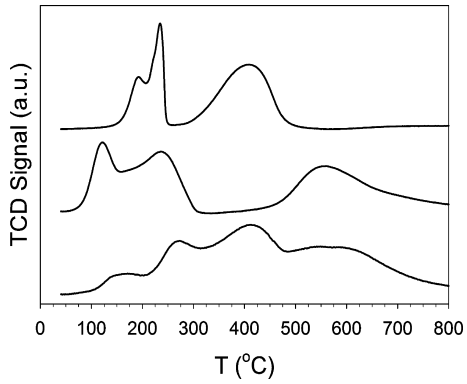

Figure 12. TPR profiles of (top) 0.2% Pt−10% Co/Al_2O_3 reference catalyst, and 0.2% Pt−10% Co/C catalysts prepared by (middle) IWI or (bottom) CVD.

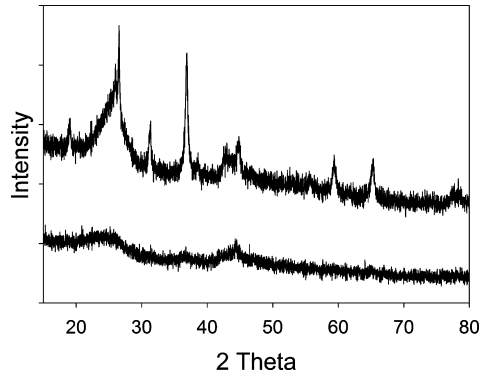

Figure 13. XRD profiles of 0.2% Pt−10% Co/C catalysts prepared by (top) IWI or (bottom) CVD.

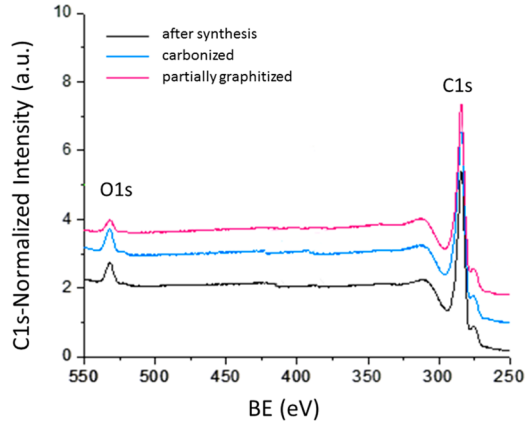

Figure 14. XPS analyses of carbon support material used for FTS.

On the other hand, the olefin selectivity for the Co/CS-CVD catalyst was lower than that of the two cobalt/alumina catalysts at similar conversion levels. An important finding of the current study reveals that Co catalysts on hydrothermal carbon supports have a higher selectivity toward oxygenate formation and, in particular, alcohols. A dependency of oxygenate selectivity with CO conversion for a typical product sample obtained over Co/CS- CVD is shown in Figure 4.

As CO conversion increased from 26 to 40%, the selectivity toward oxygenates dropped from ∼11 to ∼6.0% (Figure 4; oxygenates from both oil and water phases are included for the Co/CS-CVD catalyst). Thus, the selectivity toward oxygenates increased with increasing TOS for FT synthesis as the catalyst underwent aging. This observed change in oxygenates selectivity with CO conversion may be based on secondary reactions of olefins. A possible CO insertion[33−35] to an alkyl-metal bond (Scheme 1i) is a likely primary route of formation of oxygenates. Alternatively, Johnston and Joyner[29] proposed that oxygen containing surface species can be formed via addition of a hydroxyl group to an alkylidene species (Scheme 1ii).

The product selectivity changes may also be explained in terms of the hydrogenation activity of the cobalt-based catalyst (including catalyst deterioration over time, in combination with competitive adsorption due to overall CO conversion). It is well-known that olefins can readsorb and undergo secondary reactions such as hydrogenation, hydration, isomerization, and incorporation into a growing hydrocarbon chain, during FT synthesis. In the case of cobalt supported catalysts, because of a high hydrogenation activity compared to iron, the former produces lesser amounts of olefins. Hence, secondary reactions of olefins become less significant over cobalt. However, in the conversion range studied, the supported cobalt catalysts produce a significant (11.7−18.8%) amount of olefins, as shown in Table 1, and these might undergo secondary reactions, resulting in the formation of the observed alcohols (∼10% for Co/CS-CVD at 26.5% conversion) in the FTS product. Another important possibility is that of a CO insertion mechanism, which could be a major pathway in producing alcohols, particularly at lower CO conversion, as previously proposed by Schulz et al.,[28] for carbon-supported catalysts during FT synthesis. Figure 5 illustrates the distribution of alcohols for the Co/CS-IWI- and Co/CS-CVD catalysts.

More than 70% of the alcohols are in the carbon number range of C_1−C_3 on both of the carbon supported cobalt catalysts that were studied (again, note the difference in conversion). Methanol contributes nearly 40−50% of the total oxygenates that were formed. The difference in the oxygenate selectivity between Co/CS-CVD (∼10%) and the cobalt/alumina (2.4−5.5%) catalysts at similar conversion levels suggests that the nature of the support, in this case partially graphitized carbon nanostructures, may play a determining factor in boosting oxygenate selectivity during FTS (Table 1).

We speculated that the higher CO conversion (26.5%) and the enhanced hydrogenation activity on a per-gram catalyst basis of the carbon-supported catalyst (Co/CS-CVD) may be linked to a higher dispersion of cobalt relative to the Co/CS-IWI catalyst. Therefore, the catalyst particle size and dispersion of Co on the carbon supported catalysts were investigated by TEM. Catalyst samples were compared before and after FTS for both Co/CS-IWI and Co/CS-CVD catalysts using TEM, and the results are summarized in Figures 6−8. Prior to investigating the catalyst samples, the nanostructure of the partially graphitized carbon spheres (Figure 6) was imaged to examine the surface features of the support. The surfaces show carbon nanostructures that resemble randomly arranged ribbons or planes, the latter of which are stacked up to several layers (Figure 6). The IWI technique tended to produce isolated, larger Co clusters on the surface of the CS support, and cluster sizes up to ∼100 nm were frequently observed to extend outward from the carbon support surface (Figure 7; left column). These clusters are composed of typically ∼5 nm sized Co crystallites. In contrast, the CVD technique produced much higher dispersions of Co catalyst particles and also a more

dx.doi.org/10.1021/cs400965t | ACS Catal. 2014, 4, 1662−1672

uniform coverage on the CS support surface (Figure 7; right column).

At higher magnification, it is obvious that the primary Co crystallite size in the CVD sample is also ∼5 nm, but the particles are much less aggregated. It should be pointed out that the Co crystallite size in the CVD sample is right at the border and just below the optimum catalyst particle size suggested by others (6−8 nm[3] for some Co-FT catalysts. After FTS, the dispersion of the Co crystallites changed drastically for the IWI sample, and instead of having isolated large clusters, the entire CS spheres appear now to have been blanketed with finely dispersed Co crystallites (Figure 8; left column). It seems that the large Co-clusters became dispersed during the FT synthesis runs, which was unexpected. Rather, we expected even larger crystals through processes such as Ostwald ripening that would decrease the reactive catalyst surface area and the dispersion. The CVD catalyst sample after FT synthesis also exhibited finely dispersed Co crystallites (Figure 8; right column), but there are two main differences with the IWI sample: (1) the IWI sample has finely dispersed Co on the surface that is protruding outward, and the CVD sample has Co in close proximity to the carbon nanostructure over the entire sphere; and (2) the CVD sample displayed numerous CS spheres in which the carbon nanostructure had opened up to produce voids. Spheres are perforated and in some instances have missing sections (Figure 8; right column), but this is much less prevalent than in the case of the IWI sample.

A schematic that highlights the differences observed in TEM between IWI and CVD samples is also included in Figure 8. The higher Co dispersion by the CVD method relative to the IWI method in the as-prepared carbon supported catalysts may explain the significantly higher CO conversion observed with the CVD catalyst at similar space velocity. To help explain the physical changes in the carbon structures (voids) it will be important to investigate the presence of any carbon from the support in the FTS products, and the authors will study this aspect using isotopic labeling in a follow-up investigation to this work.

The BET surface area of the carbon support was also obtained and is very low after the hydrothermal carbons were graphitized. The corresponding BET results and PSD profiles are shown in Table 2; however, by adding the metals and calcining with inert gas, the surface area and pore volume increased significantly (i.e., by a factor of 5 to 7 times). Table 2 also includes results for the alumina support for comparison.

XANES spectra of the two different Co catalyst samples were analyzed to gain insight into the extent of Co reduction of the catalyst for the two different preparation techniques (IWI vs CVD), which can also help interpret the catalyst cluster size.[36] Figure 9 shows a comparison of the normalized XANES spectra. There is a measurable difference between the white line intensities of the CVD versus the IWI catalyst. The IWI catalyst is virtually completely reduced, whereas that of the CVD is significantly reduced but still retains an oxidized component. A linear combination XANES fitting (Figure 10) of the spectrum of the CVD catalyst with the reference compounds revealed an extent of reduction of ∼70.5% (i.e., Co metal content in a mixture of Co metal and CoO). It is well-known in FT catalysis that high extents of reduction are commonly associated with large Co particle sizes.[36]

For example, for air-calcined impregnated catalysts prepared using a strongly interacting Al_2O_3 support versus a weakly interacting SiO_2 support, a 15% Co/SiO_2 catalyst displayed more than double the extent of reduction (64% versus 30%) compared with the 15% Co/Al_2O_3-supported Co catalyst.[29] Despite this, the Al_2O_3-supported cobalt catalyst had over 3 times the active site density (66.9 μmol per gram of catalyst versus 16.9) as a result of the stabilization of a smaller cobalt cluster size (5.9 nm versus 49.7 nm). Thus, a lower extent of reduction often indicates a smaller average cluster size (in our case, for the CVD sample well dispersed ∼5 nm Co clusters), with the fraction of smallest species in strongest interaction with the support and, hence, more difficult to reduce. Another way of looking at it is that the Co/SiO_2 catalyst exhibited reduction characteristics quite similar to bulk Co_3O_4, which reduces over a narrow range at close to 300−350 °C, whereas the 15% Co/Al_2O_3 catalyst exhibited a much broader range (300−800 °C) due to smaller cobalt oxide species in strong interaction with the support.

Figure 11 shows our current results of EXAFS fittings for the carbon-supported catalysts and a powder CoO reference compound. As summarized in Table 3, the CVD catalyst exhibits a smaller average Co−Co coordination number for bonding in the metal and just slightly higher Co−O coordination. In short, the EXAFS results are consistent with a somewhat smaller average cobalt cluster size because the CVD catalyst that has Co crystallites is in greater contact with the carbon support.

TPR profiles (Figure 12) confirm a two-step reduction for Co_3O_4 in which the second step of reduction (CoO to Co^0) consumes about 3 times as much hydrogen at the first reduction step (Co_3O_4 to CoO).[31] A low-intensity broad peak was observed at higher temperatures (600 °C+) for the 0.2% Pt−10% Co/Al_2O_3 catalyst, indicating that a small fraction of the cobalt formed cobalt support compounds. Both steps of reduction are significantly facilitated with the presence of Pt promoter; it is known that bulk Co_3O_4 reduces at 300−350 °C. The support appears to react with hydrogen at higher temperature, where the rate is slow at 350 °C, peaking at 550 °C. For the CVD catalyst, the profiles for reduction of Pt and Co oxides are significantly broadened, beginning at 100 °C and complete before ∼500 °C in TPR, and a significant fraction are reduced at higher temperature than the IWI catalyst. Moreover, the peaks for CoO reduction and reaction of H_2 with the support display significant overlap. The broadening of the profiles for the reduction of cobalt oxides indicates smaller cobalt oxide crystallites in closer surface interaction with the support. This is in line with XRD results (Figure 13) for cobalt oxide size (prior to reduction) and EXAFS results for Co−O and Co−Co coordination after reduction as well as the higher white line intensity at the Co K edge for the CVD catalyst following hydrogen activation.

The XRD analysis of the IWI catalyst was conducted using Winfit: The integral breadth method for Co_3O_4 line at 2θ = 36.8° resulted in a diameter of 14.7 nm. Correcting for reduction by using a factor of 0.75 brings the average expected cobalt metal crystallite size to 11.0 nm. The line was too broad to be used in the analysis of the CVD catalyst (Figure 13), indicating finely dispersed Co oxide prior to catalyst activation.

The XPS analysis of the carbon support used in this study before FTS is shown in Figure 14 and indicates a strong signal for the oxygen O 1s peak at 533.2 (eV) for the hydrothermally derived carbon materials, even after carbonization. After partial graphitization, the oxygen O 1s peak is still present, albeit somewhat diminished.

dx.doi.org/10.1021/cs400965t | ACS Catal. 2014, 4, 1662−1672

5. CONCLUSIONS

Hydrothermal carbon spheres with partially graphitized surfaces were investigated as potential candidates for catalyst support materials for FTS and resulted in higher oxygenate selectivities for Co catalysts compared with conventional Co/alumina catalysts at similar conversion. CO conversion levels of practical interest can be achieved, but activity on a per-gram basis is strongly dependent on the resulting Co particle size on the carbon support, which in turn is greatly influenced by the method of preparation. A CVD method led to a higher CO conversion (26.5%) relative to a more traditional, evaporative method (IWI, 7.4% conversion) at similar space velocities. Detailed microscopic investigations of the fresh catalysts and those after FTS for both preparation methods revealed that the original Co particle arrangement on the carbon surfaces undergoes a change during FT synthesis, and the catalyst particles become less agglomerated. Typically, on the basis of well-known ripening processes, one would expect the exact opposite.

The carbon support structure was also altered during FTS such that the resulting carbon nanostructure formed numerous voids. We believe that the extent of the changing support structure of the carbon spheres is, at least in part, caused by a selective breakdown of nongraphitized domains, since the carbons were treated at 1900 °C, which is well below the graphitization temperature. The CVD sample, with its more finely dispersed Co particles throughout the entire carbon spheres, was found to alter the carbon structure more after FTS.

The physical breakdown of regions within the carbon support could have an effect on the dispersion of the Co catalyst particles and also on the cluster sizes, since Ostwald ripening or sintering was not observed. It will be important to also study carbon supports that are completely graphitized to see if the partial breakdown of the carbon nanostructure and formation of voids in the graphitized support also takes place and influences Co catalyst size, location and catalytic activity. Remarkably, at similar conversion levels, the 0.2% Pt−10% Co/CS-CVD catalyst produced approximately four times the amount of oxygenates as a conventional 0.5% Pt−25% Co/Al_2O_3 catalyst and double the amount of oxygenates as a similarly metal-loaded 0.2% Pt−10% Co/Al_2O_3 reference catalyst.

AUTHOR INFORMATION

Corresponding Author

*Phone: 859-257-0251. E-mail: burtron.davis@uky.edu.

Notes

The authors declare no competing financial interest.

ACKNOWLEDGMENTS

Support for this study was from the Commonwealth of Kentucky.

REFERENCES

(1) O'Brien, R. J .; Xu, J.; Bao, L. G.; Raje, S. Q.; Davis, B. H. *Appl. Catal., A* **2000**, *196*, 173−178.
(2) Zhen, Y.; Wang, Z.; Bukur, D. B.; Goodman, D. W. *J. Catal.* **2009**, *26*, 196−200.
(3) Bezemer, G. L.; Bitter, J. H.; Kuipers, H. P.; Oosterbeek, H.; Holewijn, J. E.; Xu, X.; Kapteijn, F.; van Dillen, A. J.; de Jong, K. P. *J. Am. Chem. Soc.* **2006**, *128*, 3956−64.
(4) Fu, T.; Jiang, Y.; Jv, J.; Li, Z. *Fuel Process. Technol.* **2013**, *110*, 141−149.
(5) Furimsky, E. *Carbons and Carbon Supported Catalysts in Hydroprocessing*; RSC: Cambridge, UK, 2008.
(6) Graham, U. M.; Dozier, A.; Khatri, R. A.; Bahome, M. C.; Jewell, L. L.; Mhlanga, S. D.; Coville, N. J.; Davis, B. H. *Catal. Lett.* **2009**, *129*, 39−45.
(7) Titirici, M. M.; Antonietti, M. *Chem. Soc. Rev.* **2009**, *39*, 103−16.
(8) Titirici, M. M.; Antonietti, M.; Baccile, N. *Green Chem.* **2008**, *10*, 1204−12.
(9) Sevilla, M.; Fuertes, A. *Chem.—Eur. J.* **2009**, *15*, 4195−203.
(10) Chen, C.; Sun, X.; Jiang, X.; Niu, D.; Yu, A.; Liu, Z. *Nanoscale Res. Lett.* **2009**, *4*, 971−976.
(11) Titirici, M. M. *Sustainable Carbon Materials from Hydrothermal Processes*; John Wiley & Sons: Chichester, 2013.
(12) Lipka, S. M.; Chen, R.; Swartz, C. R., Kunadian I.; Rogers, F. 222nd Meeting of the Electrochemical Society, Honolulu, Hawaii, October 7−12, 2012.
(13) Diehl, F.; Khodakov, A. Y. *Oil Gas Sci. Technol.* **2009**, *64*, 11−24.
(14) Xiaoding, X.; Doesburg, E. B. M.; Scholten, J. J. F. *Catal. Today* **1987**, *2*, 125−170.
(15) Spadaro, I.; Arena, F.; Granadeos, M. I.; Ojeda, M.; Fierro, J. I. G.; Frusteri, F. *J. Catal.* **2005**, *234*, 451−462.
(16) Gnanamani, M. K.; Ribeiro, M. C.; Ma, W.; Shafer, W. D.; Jacobs, G.; Graham, U. M.; Davis, B. H. *Appl. Catal., A* **2011**, *393*, 17−23.
(17) Gong, Y. F.; Liu, S. H.; Guo, H. J.; Hu, T. G.; Zhou, L. B. *Appl. Therm. Eng.* **2007**, *27*, 202−207.
(18) Reuel, R. C.; Bartholomew, C. H. *J. Catal.* **1984**, *85*, 63−77.
(19) Espinoza, R. L.; Visagie, J. L.; van Berge, P. J.; Bolder, F. H. U.S. Patent 55,733,839, 1998.
(20) Jacobs, G.; Alvarez, W. E.; Resasco, D. E. *Appl. Catal., A* **2001**, *206*, 267−282.
(21) Jacobs, G.; Ghadiali, F.; Pisanu, A.; Borgna, A.; Alvarez, W. E.; Resasco, D. E. *Appl. Catal., A* **1999**, *188*, 79.
(22) Berg, E. W.; Hartlage, F. R., Jr. *Anal. Chim. Acta* **1965**, *33*, 173−181.
(23) Ballatreccia, M.; Zanoni, R.; Dossi, C.; Psaro, R.; Recchia, S.; Vlaic, G. *J. Chem. Soc., Faraday Trans.* **1995**, *91*, 2045−49.
(24) Jacobs, G.; Ghadiali, F.; Pisanu, A.; Padro, C. L.; Borgna, A.; Alvarez, W. E.; Resasco, D. E. *J. Catal.* **2000**, *191*, 116−127.
(25) Resasco, D. E.; Padro, C. L.; Jacobs, G.; Liu, H.-Y. U.S. Patents 6,063,724, 2000; 6,096,193, 2000; and 6,096,675, 2000.
(26) Tiedtke, D. B.; Cheung, T-T.P.; Resasco, D. E.; Jacobs, G. U.S. Patent 6,406,614, 2001.
(27) Diets, W. A. *J. Chromatogr. Sci.* **1967**, *5*, 68−71.
(28) Ressler, T. *J. Synchrotron Radiat.* **1998**, *5*, 118−122.
(29) Ravel, B. *J. Synchrotron Radiat.* **2001**, *8*, 314−316.
(30) Newville, M.; Ravel, B.; Haskel, D.; Rehr, J. J.; Stern, E. A.; Yacoby, Y. *Physica B* **1995**, *154*, 208−209.
(31) Jacobs, G.; Ji, Y.; Davis, B. H.; Cronauer, D. C.; Kropf, A. J.; Marshall, C. L. *Appl. Catal., A* **2007**, 177−191.
(32) Gnanamani, M. K.; Jacobs, G.; Hamdeh, H. H.; Shafer, W. D.; Davis, D. H. *Catal. Today* **2013**, *207*, 50−56.
(33) Schweicher, J.; Bundhoo, A.; Kruse, N. *J. Am. Chem. Soc.* **2012**, *134*, 16135−38.
(34) Schulz, H.; Riedel, T.; Schaub, G. *Top. Catal.* **2005**, *32*, 117−124.
(35) Johnston, P.; Joyner, R. W. *Stud. Surf. Sci. Catal.* **1993**, *75*, 165−180.
(36) Jacobs, G.; Das, T. K.; Zhang, Y.-Q.; Li, J.; Racoillet, G.; Davis, B. H. *Appl. Catal., A* **2002**, *233*, 263−281.